

Supporting Information

Magneto-chiral Dichroism in Mixed (Phthalocyaninato)(Porphyrinato) Rare Earth Triple-Decker SMMs

Kang Wang,[†] Suyuan Zeng,[‡] Hailong Wang,[†] Jianmin Dou,[‡] and Jianzhuang Jiang^{†,*}

Experimental Section

General. *n*-Octanol was distilled from sodium. Column chromatography was carried out on silica gel (Merck, Kieselgel 60, 70-230 mesh) with the indicated eluents. $\text{Y}(\text{acac})_3 \cdot n\text{H}_2\text{O}$,^{S1} $\text{Dy}(\text{acac})_3 \cdot n\text{H}_2\text{O}$,^{S1} (*R*)/(*S*)- $\text{H}_2[\text{Pc}(\text{OBNP})_4]$,^{S2} and H_2TCIIPP ^{S3} were prepared according to the published procedures. All other reagents and solvents were used as received.

¹H NMR spectra were recorded on a Bruker DPX 400 spectrometer in CDCl_3 . Spectrum was referenced internally using the resonances of SiMe_4 ($\delta = 0$ for ¹H NMR). Electronic absorption spectra were recorded on a Hitachi U-4100 spectrophotometer. IR spectra were recorded as KBr pellets using a Bruker Tensor 37 spectrometer with 2 cm^{-1} resolution. MALDI-TOF mass spectra were taken on a Bruker BIFLEX III ultrahigh-resolution Fourier transformion cyclotron resonance (FT-ICR) mass spectrometer with alpha-cyano-4-hydroxycinnamic acid as matrix. Elemental analyses were performed on an Elementar Vario El III. CD spectra were recorded using a Jasco J-810 spectrodichrometer. MCD and magneto-chiral dichroism spectra measurements were made on a JASCO J-815 spectropolarimeter in the presence of magnetic field (1.6 T) with both parallel and antiparallel fields. For magneto-chiral dichroism spectra measurements, using a reported method,^{S4}, we measured the absorbance in directions parallel to **B** and then the absorbance in

directions antiparallel to **B** in the region of 350-450 nm point-by-point at 0.5 nm. Subsequently, we measured the antiparallel absorbance first and then the parallel absorbance. By repeating this procedure 20 times, the data was accumulated, and then the averaged magneto-chiral dichroism spectra were obtained from the difference between the parallel and antiparallel absorption spectra. Crystal data for (*R*)/(*S*)-**1**, and (*R*)/(*S*)-**2** were determined by X-ray diffraction analysis at 150 K using Oxford Diffraction Gemini E system with Cu_{Kα} radiation $\lambda = 1.5418 \text{ \AA}$, and details of the structure refinement are given in Table S2 (Supporting Information). CCDC number: 950171-950174 containing the supplementary crystallographic data for this paper can be obtained free of charge from the Cambridge Crystallographic Data Centre *via* www.ccdc.cam.ac.uk/data_request/cif. Electrochemical measurements were carried out with a BAS CV-50W voltammetric analyzer. The cell comprised inlets for a glassy-carbon-disk working electrode of 2.0 mm in diameter and a silver-wire counter electrode. The reference electrode was Ag/Ag⁺, which was connected to the solution by a Luggin capillary whose tip was placed close to the working electrode. It was corrected for junction potentials by being referenced internally to the ferrocenium/ferrocene (Fe⁺/Fe) couple ($E_{1/2}[\text{Fe}^+/\text{Fe}] = 501 \text{ mV vs SCE}$). Typically, a 0.1 mol dm⁻³ solution of [Bu₄N][ClO₄] in CH₂Cl₂ containing 0.5 mmol dm⁻³ of sample was purged with nitrogen for 10 min. The voltammograms were then recorded at ambient temperature. The scan rate was 40 and 10 mVs⁻¹ for CV and DPV,

respectively.

Synthesis of (*R*)/(*S*)-{M₂[Pc(OBNP)₄](TCIPP)₂} (M = Y, Dy) (1, 2). A mixture of M(acac)₃·nH₂O (0.080 mmol), (*R*)/(*S*)-H₂[Pc(OBNP)₄] (65.7 mg, 0.040 mmol), and H₂TCIPP (60.2 mg, 0.080 mmol) in dry *n*-octanol (3.0 mL) was heated to reflux under nitrogen for 4 h. After being cooled to room temperature, the volatiles were removed under reduced pressure and the residue was purified by chromatography on a silica-gel column with CHCl₃ as the eluent to give a dark green band. Further repeated biobead chromatography followed by recrystallization from toluene and methanol gave pure target mixed (phthalocyaninato)(porphyrinato) rare earth triple-decker complexes with the yield of ca. 50%. ¹H NMR (400 MHz, CDCl₃) for **1**, δ: 9.36 (s, 8H, *Pc*-α-*H*), 8.56 (m, 8H, *Ph*), 8.27 (d, 8H, *Ph*), 8.19 (d, 8H, *Ph*), 7.93 (d, 8H, *Ph*), 7.72 (m, 8H, *Ph*), 7.60-7.70 (m, 16H, *Ph*), 7.65 (d, 8H, *Ph*), 7.46, (d, 8H, *Por*-β-*H*), 7.35, (d, 8H, *Por*-β-*H*), 7.11, (m, 8H, *Ph*), and 5.95 (m, 8H, *Ph*). MS (MALDI-TOF) for **1**: Calcd. for Y₂C₂₀₀H₁₀₄Cl₈N₁₆O₈Li [M+Li]⁺ 3320.4; found *m/z* 3320.5. Anal. Calcd. for (*R*)-**1**: Y₂C₂₀₀H₁₀₄Cl₈N₁₆O₈·3C₆H₈·5H₂O: C 71.53, H 3.84, N 6.18; Found: C 71.46, H 4.25, N 5.88. Anal. Calcd. for (*S*)-**1**: Y₂C₂₀₀H₁₀₄Cl₈N₁₆O₈·2CH₃OH: C 71.68, H 3.34, N 6.62; Found: C 71.85, H 3.83, N 6.33. MS (MALDI-TOF) for **2**: Calcd. for Dy₂C₂₀₀H₁₀₄Cl₈N₁₆O₈Li [M+Li]⁺ 3320.4; found *m/z* 3320.5. Anal. Calcd. for (*R*)-**2**: Dy₂C₂₀₀H₁₀₄Cl₈N₁₆O₈·3C₆H₈·5H₂O: C 68.94, H 3.66, N 5.90; Found: C 68.90, H 3.95, N 5.98. Anal. Calcd. for (*S*)-**2**: Dy₂C₂₀₀H₁₀₄Cl₈N₁₆O₈·3C₆H₈·3CH₃OH:

C 69.77, H 3.71, N 5.89; Found: C 69.52, H 4.18, N 6.02.

Electrochemical properties. The redox behavior of both **1** and **2** was studied by cyclic voltammetry (CV) and differential pulse voltammetry (DPV) in CH₂Cl₂. As shown in Fig. S8 (Supporting Information), within the electrochemical window of CH₂Cl₂, four quasi-reversible one-electron oxidations and up to three quasi-reversible one-electron reductions were revealed for both compounds. All the processes can be attributed to the successive removal of an electron and addition of an electron to the ligand-based orbitals as the oxidation state of the central tervalent rare earth metals in the triple-decker complexes does not change. The half-wave potentials are summarized in Table S5 (Supporting Information). The potential difference between the first oxidation and first reduction processes in the yttrium analogue **1** is significantly smaller than that revealed for [(TCIPP)Y(Pc)Y(TCIPP)]^{S5} due to the introduction of the peripherally attached binaphthyl substituents at the phthalocyanine ring. This result is in agreement with the red-shift of the lowest energy absorption band in the near IR range from 995 nm for [(TCIPP)Y(Pc)Y(TCIPP)]^{S5} to 1006 nm for **1**. This is also true for the dysprosium analogue **2**.

References

- [S1] J. G. Stites, C. N. McCarty and L. L. Quill, *J. Am. Chem. Soc.* **1948**, 70, 3142-3143.

- [S2] (a) K. Wang, D. Qi, H. Wang, W. Cao, W. Li and J. Jiang, *Chem. Eur. J.* **2012**, 18, 15948 -15952; (b) K. Wang, H. Wang, J. Mack, W. Li, N. Kobayashi and J. Jiang, *Acta Chim. Sinica* **2012**, 70, 1791-1797.
- [S3] G. H. Barnett, M. F. Hudson and K. M. Smith, *J. Chem. Soc. Perkin Trans. I* 1975, 1401-1403.
- [S4] (a) G. L. J. A. Rikken and E. Raupach, *Phys. Rev. E* **1998**, 58, 5081-5084; (b) C. Koerdt, G. Duchs and G. L. J. A. Rikken, *Phys. Rev. Lett.* **2003**, 91, 073902; (c) Y. Kitagawa, H. Segawa and K. Ishii, *Angew. Chem.* **2011**, 123, 9299-9302; (d) Y. Kitagawa, T. Miyatakeb and K. Ishii, *Chem. Commun.* **2012**, 48, 5091-5093; (e) S. Bordács, I. Kézsmárki, D. Szaller, L. Demkó, N. Kida, H. Murakawa and Y. Onose, *Nature Physics* **2012**, 8, 734-738.
- [S5] X. Sun, R. Li, D. Wang, J. Dou, P. Zhu, F. Lu, C. Ma, Ch-F. Choi, D. Y. Y. Cheng, D. K. P. Ng, N. Kobayashi and J. Jiang, *Eur. J. Inorg. Chem.*, **2004**, 19, 3806-3813.

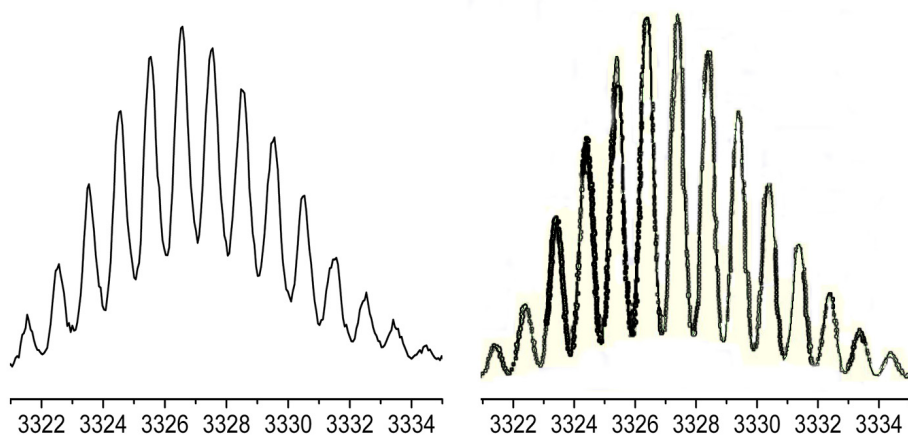


Fig. S1. Experimental (left) and simulated isotopic (right) pattern for the molecular ion of **1** shown in the MALDI-TOF mass spectrum

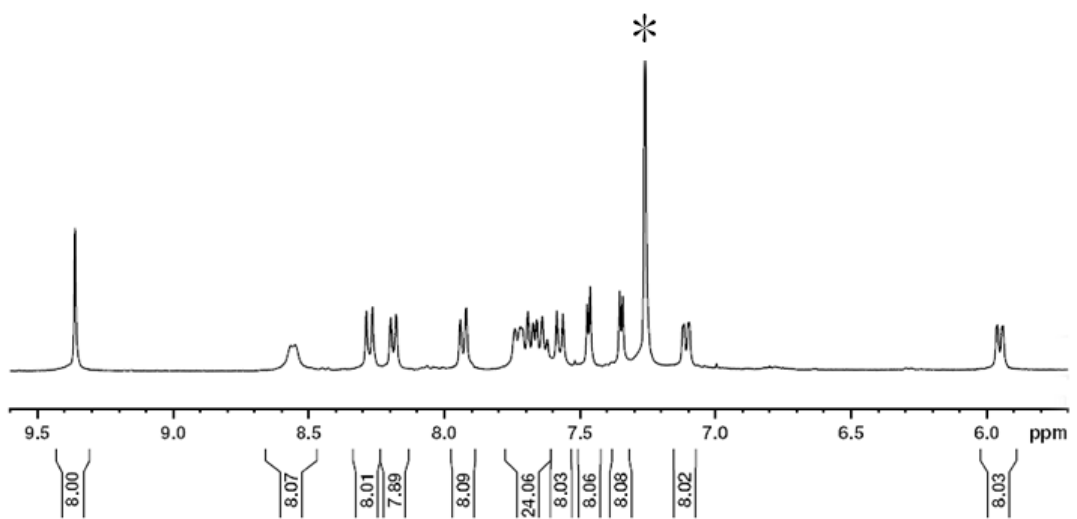


Fig. S2. ^1H NMR and ^1H - ^1H COSY spectra of **1** recorded in CDCl_3 at 293 K. * denotes a solvent impurity.

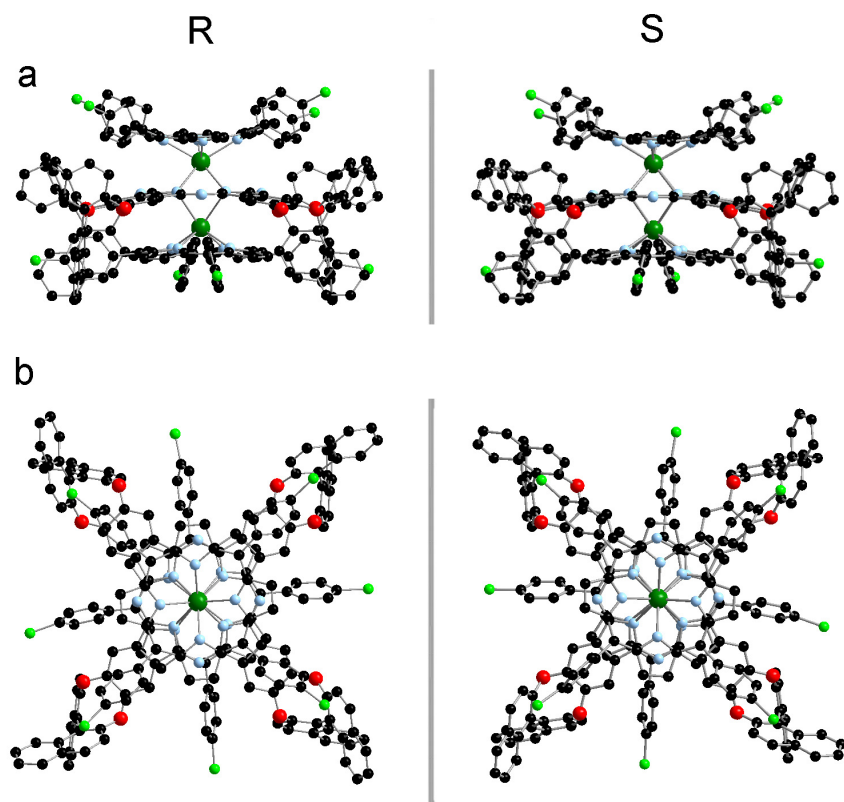


Fig. S3. Molecular structure of **1** in side view and top view with all hydrogen atoms omitted for clarity [**Y(III)** dark green, C black, N pale blue, O red, Cl light green].

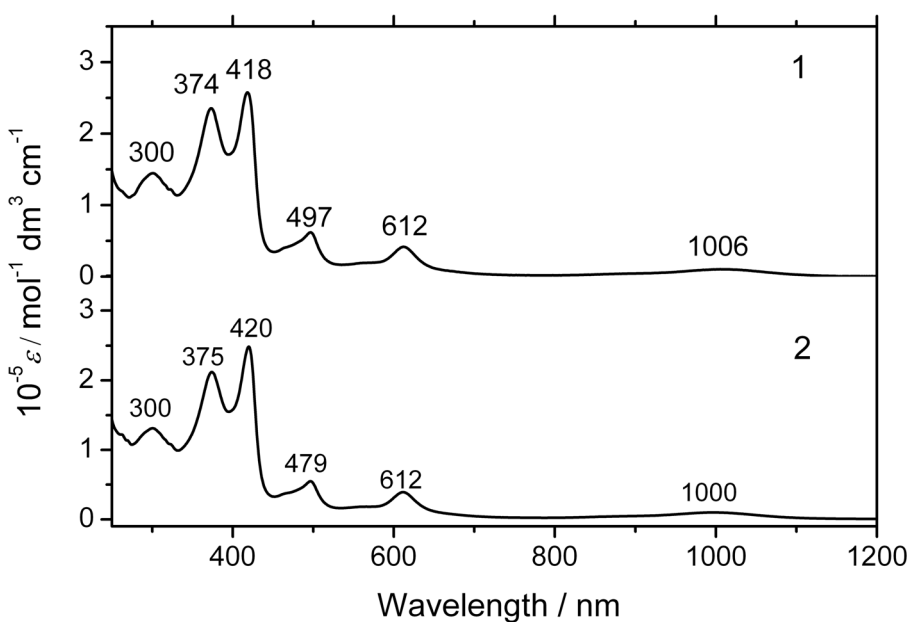


Fig. S4. Electronic absorption spectra of **1** and **2**.

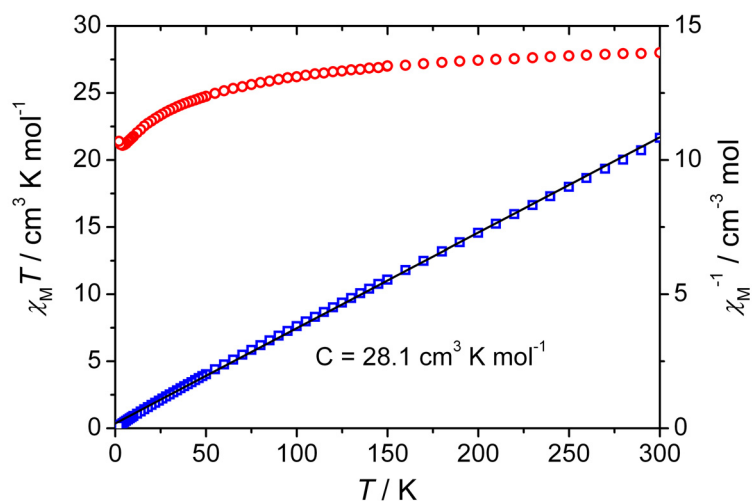


Fig. S5. Temperature (T) dependence of $\chi_m T$ and $1/\chi_m$ for powder samples of **2** at 1000 Oe. In the $1/\chi_m$ vs T plot, the black solid line represents a linear fit of the all data.

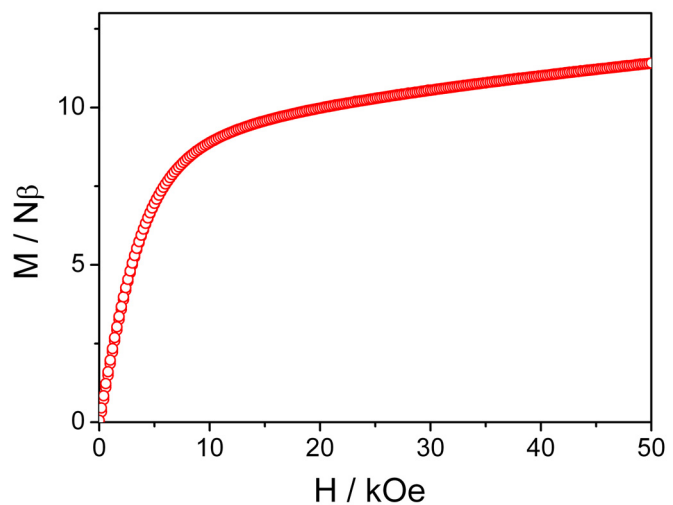


Fig. S6. The M vs. H curves for **2** at 2.0 K.

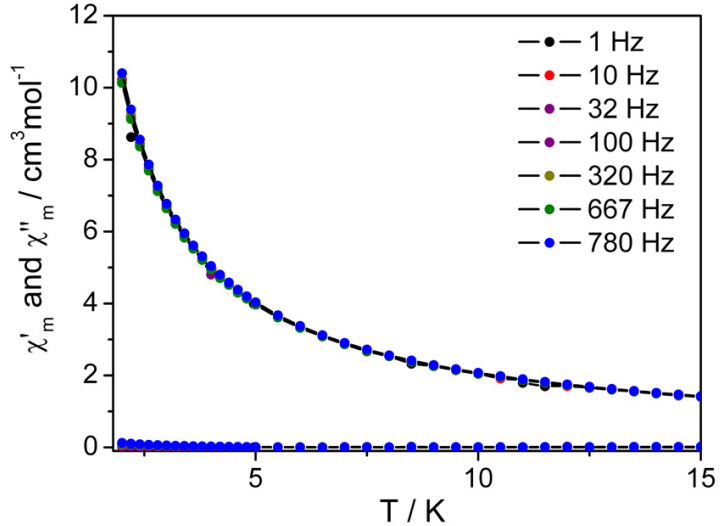


Fig. S7. Temperature dependence of out-of phase (χ'') and the in-phase (χ') ac susceptibility of **2** in dc fields of 0 Oe.

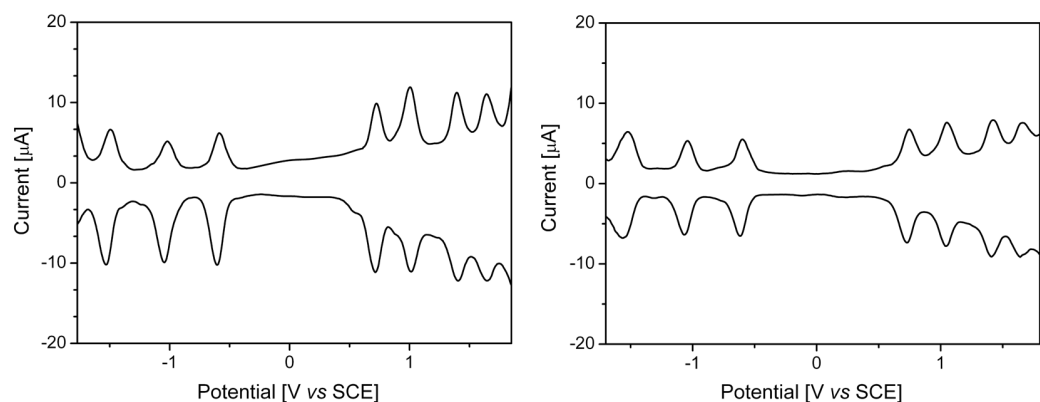


Fig. S8. Differential pulse voltammetry of **1** (left) and **2** (right) in CH_2Cl_2 containing 0.1 mol dm^{-3} $[\text{NBu}_4]\text{[ClO}_4]$ at scan rates of 10 mV s^{-1} .

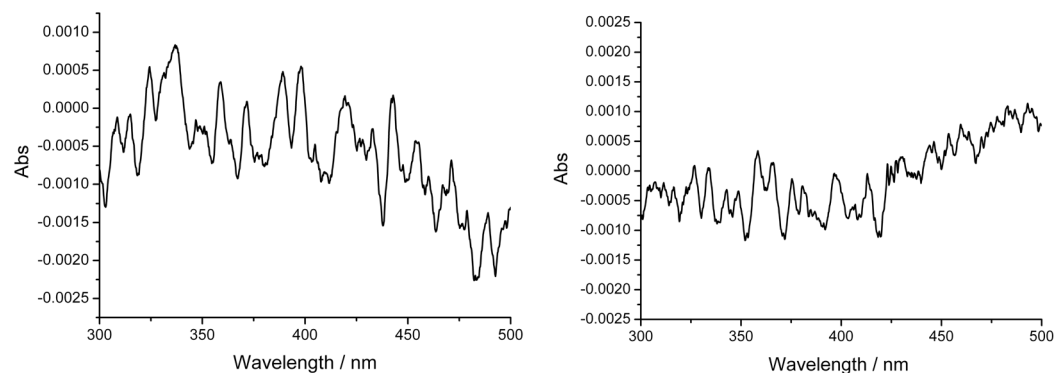


Fig. S9. Left: The baseline of the electronic absorption spectra of JASCO J-815 spectropolarimeter in the range of 300-500 nm in CHCl₃. Right: The difference between two contiguous electronic absorption measurements of (*S*)-2 when the absorbance at 418 nm is about 0.8 in CHCl₃.

Table S1. ^1H NMR data (δ) for **1** recorded in CDCl_3 at 293 K.

	Signals for TClPP		Signals for $\text{Pc}(\text{OBNP})_4$	
	H_β	H_{aryl}	H_α	H_{OBNP}
1	7.46 (8 H) 7.35 (8 H)	8.56 (8 H), 8.27 (8 H), 7.11 (8 H), 5.95 (8 H)	9.36 (8 H)	8.19 (8 H), 9.23 (8 H), 7.60-7.70 (16 H), 7.72 (8 H), 7.57 (8 H)

Table S2. Crystal data and structure refinements of (*R*)- and (*S*)-enantiomers for both **1** and **2**.

Compound	(<i>R</i>)- 1	(<i>S</i>)- 1	(<i>R</i>)- 2	(<i>S</i>)- 2
formula	C ₂₂₂ H ₁₃₂ Cl ₈ N ₁₆ O ₉ Y ₂	C ₂₄₂ H ₁₅₁ Cl ₈ N ₁₆ O ₈ Y ₂	C ₂₀₀ H ₁₀₄ Cl ₈ N ₁₆ O ₈ Dy ₂	C ₂₀₁ H ₁₀₈ Cl ₈ N ₁₆ O ₉ Dy ₂
fw	3628.86	3872.21	3467.59	3499.63
crystal system	Monoclinic	Monoclinic	Monoclinic	Monoclinic
space group	<i>C</i> ₂	<i>C</i> ₂	<i>C</i> ₂	<i>C</i> ₂
<i>a</i>	44.5471(8)	44.5179(6)	44.5558(12)	44.4004(10)
<i>b</i>	22.4094(5)	22.3153(3)	22.3269(15)	22.2600(6)
<i>c</i>	22.6423(4)	22.6523(2)	22.6969(6)	22.6346(4)
α	90.00	90.00	90.00	90.00
β	94.056(2)	94.2090(10)	94.091(2)	94.147(2)
γ	90.00	90.00	90.00	90.00
<i>V</i>	22546.6(8)	22442.8(5)	22521.2(17)	22312.4(9)
<i>Z</i>	4	4	4	4
θ range (deg)	3.00-60.00	3.00-60.00	3.00-60.00	2.91-60.00
<i>F</i> calcd (g/cm ³)	1.069	1.146	1.023	1.042
μ (mm ⁻¹)	1.988	2.024	4.770	4.822
F(000)	7448	7972	6992	7064
R ₁ (<i>I</i> >2 <i>θ</i>)	0.1255	0.1046	0.2652	0.1141
R _{w2} (<i>I</i> >2 <i>θ</i>)	0.3459	0.3018	0.3444	0.3329
R _{w2} for all	0.3718	0.3160	0.4655	0.3094
<i>GOF</i> on F ²	1.156	1.211	1.451	1.064
CCDC number	950171	950173	950172	950174

Table S3. Comparison of the structural data for **1** and **2**.

	1^c	2^c
average M ₁ /M ₂ –N(TClPP) bond distance [Å]	2.392 / 2.355	2.394 / 2.349
average M ₁ /M ₂ –N[Pc(OBNP) ₄] bond distance [Å]	2.575 / 2.778	2.573 / 2.794
M ₁ /M ₂ –N ₄ (TClPP) plane distance [Å]	1.196 / 1.161	1.213 / 1.180
M ₁ /M ₂ –N ₄ [Pc(OBNP) ₄] or Pc plane distance [Å]	1.695 / 2.009	1.692 / 2.014
interplanar distance [Å]	2.906 / 3.210	2.879 / 3.208
M ₁ –M ₂ distance [Å]	3.708	3.706
dihedral angle between the N ₄ (TClPP) and N ₄ [Pc(OBNP) ₄] mean planes.	0.70 / 0	0.63 / 1.55
average dihedral angle ϕ for the TClPP ring [°] ^a	13.14 / 12.68	12.60 / 12.45
dihedral angle ϕ for the Pc(OBNP) ₄ ring [°] ^a	8.58	9.22
average twist angle [°] ^b	41.5 / 6.9	42.3 / 7.0

^aThe average dihedral angle of the individual pyrrole or isoindole ring with respect to the corresponding N₄(TClPP) or N₄[Pc(OBNP)₄] mean planes. ^bDefined as the rotation angle of one macrocycle away from the eclipsed conformation of the two macrocycles. ^cThe date are mean value of those for two enantiomers.

Table S4. Electronic absorption data for **1** and **2** in CHCl₃.

Compound	λ_{max} nm ⁻¹ (log ϵ)					
1	300 (5.16)	375 (5.37)	418 (5.41)	497 (4.79)	612 (4.62)	1006 (4.01)
2	300 (5.16)	375 (5.33)	420 (5.40)	497 (4.74)	612 (4.59)	1000 (4.00)

Table S5. Half-wave redox potentials of binuclear phthalocyanine involved sandwich-type rare earth complexes **1** and **2** in CH₂Cl₂ containing 0.1 mol dm⁻³ TBAP.

	Oxd ₄	Oxd ₃	Oxd ₂	Oxd ₁	Red ₁	Red ₂	Red ₃	ΔE _{1/2}
1	+1.65	+1.40	+1.01	+0.72	-0.60	-1.03	-1.52	1.32
2	+1.66	+1.41	+1.04	+0.73	-0.61	-1.05	-1.54	1.34